Published by :
https://www.ijert.org/
An International Peer-Reviewed Journal

International Journal of Engineering Research & Technology (IJERT)
ISSN: 2278-0181
Vol. 14 Issue 12 , December - 2025

Comparative Evaluation of Slope Reinforcement Techniques under Pseudo-Static Unsaturated and Rainfall Conditions

Md Aadil Arfin
Department of Civil Engineering, Jamia Millia Islamia,
New Delhi – 110025

Syed Mohammad Abbas
Department of Civil Engineering, Jamia Millia Islamia,
New Delhi - 110025

Abstract - **This study evaluates the combined effects of rainfall infiltration and pseudo-static seismic loading on the stability of an unsaturated silty soil slope, using an unreinforced baseline condition for comparison. The baseline slope is subsequently reinforced with soil nails, geogrid layers, and Vetiver grass (*Chrysopogon zizanioides*) roots to assess the relative effectiveness of each stabilization technique. Rainfall-induced infiltration was modelled to capture reductions in matric suction and the associated loss of shear strength, following which pseudo-static horizontal acceleration coefficients were applied to evaluate seismic response. Key parameters examined include factor of safety, deformation patterns, and failure mechanisms for the baseline and reinforced cases. Results indicate that rainfall significantly weakens the baseline slope prior to seismic loading, thereby increasing its vulnerability to earthquake-induced deformation. Soil nailing and geogrid reinforcement provide comparable improvements in the factor of safety after rainfall, with both techniques effectively controlling deformation. Vetiver roots enhance near-surface resistance but are less effective under stronger pseudo-static loading. These findings highlight the importance of considering both rainfall-induced weakening and seismic effects when selecting reinforcement methods for unsaturated slopes.**

Keywords: Soil nailing, Slope stability, Pseudo-static analysis, Unsaturated soil, Rainfall infiltration, Finite element modelling

I. INTRODUCTION

Slope stability under seismic loading is a critical concern in geotechnical engineering, particularly for man-made slopes such as road and railway embankments, excavated cuttings, and engineered fills. These slopes often remain in an unsaturated condition, and their behaviour is strongly influenced by rainfall infiltration [1]. Rainfall reduces matric suction and, consequently, the shear strength of the soil, making slopes more susceptible to failure if an earthquake occurs during or shortly after wet conditions. Therefore, assessing the combined effects of rainfall-induced suction loss and seismic loading is crucial for reliable stability evaluation in unsaturated soils. In this study, static effects are not considered, and only the seismic response is examined. The pseudo-static method provides a practical and widely used approach for representing seismic loading in slope stability analysis by applying equivalent horizontal acceleration coefficients. This approach has been widely used in engineering practice for evaluating seismic slope stability due to its simplicity and reasonable accuracy for design-level assessments [2]. However, the performance of reinforced unsaturated slopes under such conditions depends not only on seismic forces but also on the pore-water pressure changes caused by rainfall. Ignoring rainfall effects can lead to an overestimation of slope safety during earthquakes.

In this context, the present study investigates the pseudo-static stability of an unsaturated silty soil slope after rainfall infiltration. Three reinforcement techniques, namely soil nailing, geogrid reinforcement, and Vetiver grass roots, are evaluated to assess their effectiveness in improving seismic stability. Soil nails act as deep structural inclusions, geogrids provide tensile resistance and enhance load distribution, and Vetiver roots improve shallow strength and erosion resistance.

The aim of this study is to provide a comparative assessment of three slope reinforcement techniques, namely soil nailing, geogrid reinforcement, and Vetiver grass roots, under combined rainfall infiltration and pseudo-static seismic loading. The evaluation focuses on variations in factor of safety, deformation characteristics, and plastic strain development in order to understand the stability response and failure behaviour of reinforced unsaturated slopes. The study helps in selecting effective reinforcement methods for slopes under rainfall and seismic conditions.

II. MATERIALS AND METHODS

A. Materials

The numerical analysis incorporated four components including the soil, soil nails, geogrid, and the Vetiver root system. The mechanical and physical properties of the soil are presented in Table 1, while the properties of the reinforcement elements are summarized in Table 2. Soil parameters were used in effective stress form, while the reinforcement characteristics were obtained from relevant literature and manufacturer specifications. The soil behaviour was represented using the Mohr–Coulomb constitutive model, which is commonly applied in slope stability studies because of its simplicity and ability to describe shear failure [3]. The required input parameters, namely effective cohesion (c'), friction angle (ϕ'), Young's

International Journal of Engineering Research & Technology (IJERT)
ISSN: 2278-0181
Vol. 14 Issue 12 , December - 2025

modulus (E), and effective Poisson's ratio (ν′) are summarized in Table 1.

TABLE 1. SOIL PROPERTIES ADOPTED IN THE STUDY

Material	Property	Symbol	Value	Unit
Soil	Unit weight	γ	20	kN/m³
	Effective Cohesion	c	10	kPa
	Effective Friction angle	φ	20	°
	Young's modulus	E	7500	kPa
	Effective Poisson's ratio	ν	0.35	–
	Saturated permeability	k_{sat}	1×10^{-6}	m/sec

TABLE 2. REINFORCEMENT PROPERTIES TAKEN FOR CONSIDERATION

Material	Property	Symbol	Value	Unit
Soil Nail	Density	ρ	7850	kg/m³
	Young's modulus	E	2×10^{8}	kPa
	Yield stress	f_y	500	MPa
	Poisson's ratio	ν	0.3	–
Geogrid	Density	ρ	950	kg/m³
	Young's modulus	E	1300	MPa
	Poisson's ratio	ν	0.3	–
Vetiver roots	Density	ρ	900	kg/m3
	Mean Diameter	d	0.8	mm
	Root Area Ratio	RAR	0.025	-

Unsaturated soil behaviour was represented using the extended effective stress concept, in which matric suction contributes to the effective stress [4].

$$\sigma' = (\sigma - u_a) + \chi(u_a - u_w)$$

where σ' is the effective stress, σ is the total stress, u_a and u_w are the pore-air and pore-water pressures, and χ is the effective stress parameter. In accordance with [5], the χ parameter was defined as the degree of saturation, ensuring that the influence of matric suction on shear strength decreases progressively and becomes zero at full saturation.

Rainfall effects were incorporated through the Soil Water Characteristic Curve (SWCC) and the corresponding permeability function published in [6]. In their work, these hydraulic relationships were obtained by fitting experimental data. In the present study, the curves were not recalibrated; instead, they were digitized directly from the published figures. Although minor deviations may occur due to digitization, the overall trends were preserved, and the interpreted suction–saturation and saturation–permeability data were implemented in ABAQUS as tabulated input. This approach ensured a realistic representation of rainfall-induced changes in the unsaturated silty soil. The adopted curves are presented in Fig. 1 and Fig. 2.

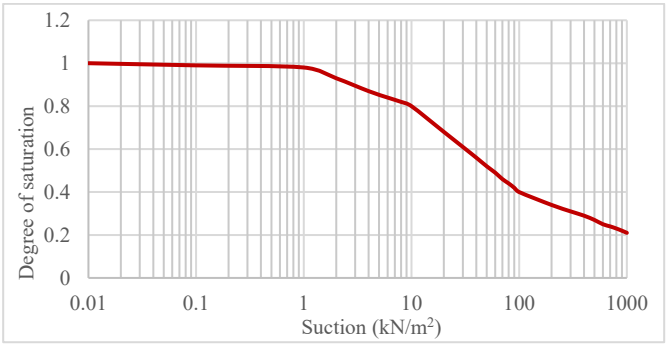

Fig. 1 Soil Water Characteristic Curves for silt

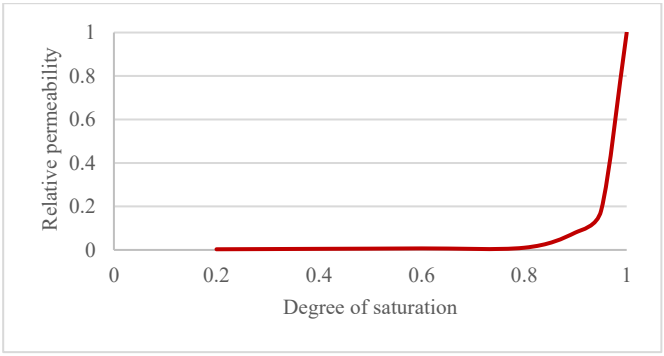

Fig. 2 Relative permeability curve of the soil as a function of degree of saturation

B. Geometry

For the numerical analysis, a representative manmade slope of approximately 10 m height was adopted and analysed under plane-strain conditions using 8-node biquadratic plane strain elements with coupled pore-pressure degrees of freedom (CPE8P). The configuration comprises a steeply inclined slope face with a finite crest width and a horizontal bench at the toe, forming a configuration commonly adopted in numerical stability studies of engineered slopes. The geometry was kept fixed for all analyses and is illustrated schematically in Fig. 3.

International Journal of Engineering Research & Technology (IJERT)
ISSN: 2278-0181
Vol. 14 Issue 12 , December - 2025

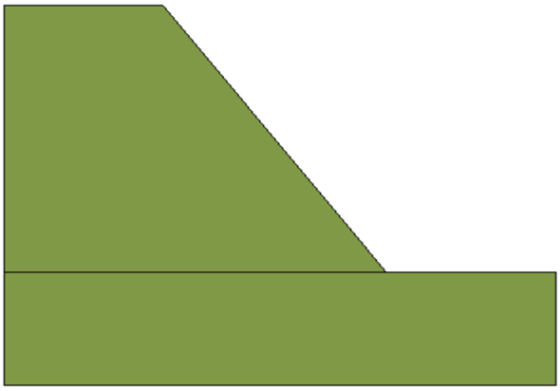

Fig. 3 Schematic representation of the slope configuration used in the numerical modelling

C. Boundary conditions

The bottom boundary of the model was fixed, preventing both horizontal and vertical displacements, while the vertical side boundaries were restrained horizontally but permitted vertical movement. Rainfall infiltration was imposed as a flux boundary condition along the exposed slope surface, with the applied flux taken as a suitable fraction of the saturated hydraulic conductivity. To simulate drainage conditions, a small outlet was incorporated at the slope base by prescribing a zero-pore pressure boundary, thereby allowing unrestricted drainage during infiltration. An initial geostatic step was executed to establish the in-situ stress equilibrium prior to the application of subsequent loading.

D. Loading conditions

Self-weight of the soil mass was simulated by applying gravitational loading over the entire domain. Pedestrian loading at the slope crest was idealized as a uniformly distributed surface load of 5 kPa. This value corresponds to the crowd loading intensity specified for footways in IRC:6-2017 and was adopted here as a conservative representation of maximum possible pedestrian occupancy at the crest [7]. The slope was further subjected to rainfall infiltration over a 48-hour period. The rainfall intensity was prescribed as a fraction of the saturated hydraulic conductivity of the soil, such that the applied rate remained slightly below the infiltration capacity. This approach replicates near-saturated field conditions without immediate surface runoff, thereby enabling progressive pore-water pressure build-up within the slope, a key factor in evaluating rainfall-induced instability. The rainfall pattern was defined as linearly increasing during the first 6 hours, remaining constant for the following 36 hours, and decreasing linearly over the final 6 hours.

Seismic loading was simulated using the pseudo-static approach, in which a constant horizontal body force corresponding to a seismic coefficient of $K_h = 0.15$ was applied after rainfall-induced pore-pressure redistribution. The selected value represents approximately 50% of the expected peak ground acceleration for moderate-to-high seismic regions. IS 1893 (Part 1): 2016 was used solely to define the regional seismic hazard through seismic zone factors and design ground acceleration [8]. The choice of the pseudo-static coefficient follows established geotechnical practice, wherein a reduced fraction of the peak ground acceleration is adopted to represent average seismic inertial effects while avoiding excessive conservatism [9].

Only the horizontal seismic component was considered in the pseudo-static analysis, as it primarily governs slope instability through shear deformation. The vertical component was not included, since its influence in pseudo-static slope stability analyses is generally secondary and inconsistent, primarily affecting normal stresses rather than driving shear failure [9]. Slope stability was evaluated under pseudo-static loading conditions, with and without rainfall infiltration.

E. Numerical Modelling Procedure

The numerical analysis was conducted in ABAQUS, with soil behaviour represented by the Mohr–Coulomb constitutive model, a widely adopted framework for slope stability studies. Shear strength was defined in terms of effective stress parameters (c′ and φ′), while elastic properties were characterized by Young's modulus (E) and the effective Poisson's ratio (ν′). The initial water content of the soil was maintained at 15%, which corresponded to the starting point on the SWCC and defined the initial matric suction condition for the unsaturated slope prior to rainfall infiltration. Unsaturated soil response was modelled using the Soil Water Characteristic Curve (SWCC) coupled with a permeability–saturation data, capturing the variation of suction, saturation, and hydraulic conductivity under rainfall infiltration.

The soil nails were modelled as linear-elastic beam elements embedded within the soil mass to allow the transfer of axial and bending forces from the nails into the surrounding ground, which is essential for capturing the composite action that provides slope reinforcement [10]. Each nail had a diameter of 20 mm, with lengths ranging from 3-5 m depending on their position along the slope to ensure they extended beyond the potential slip surface. The reinforcement was installed at an inclination of 36.87° to the horizontal, corresponding to a perpendicular orientation to the slope face, and the spacing followed the adopted reinforcement layout. The nail head was idealized at the slope face using a short line element with an equivalent square plate representation to account for nail head–facing load transfer.

The geogrid reinforcement was modelled using truss elements, which carry only axial tensile forces and do not resist bending; this approach is appropriate because geogrids primarily function as tensile reinforcement in soil. Only the density and Young's modulus of the polypropylene (PP) geogrid were taken directly from the range reported in the literature [11] and are listed in Table 2. Since Poisson's ratio was not reported, a representative value of 0.30 was adopted for polypropylene geosynthetics, which lies within the commonly reported range (0.25–0.35) in the literature as

International Journal of Engineering Research & Technology (IJERT)
ISSN: 2278-0181
Vol. 14 Issue 12 , December - 2025

reported by [12]. The analysis was performed under 2D plane-strain conditions; therefore, a uniaxial geogrid representation was adopted. Although the reference source reports tensile strengths at 5% strain and at ultimate strain, the present application involves a lightly loaded slope, where the mobilised strains are expected to remain small. Accordingly, a working-strain tensile strength of 20 kN/m at 2.5% strain was adopted, as this lies within the typical serviceability strain range (2–5%) for polypropylene geogrids reported in the literature [12]. Each geogrid layer was represented by truss elements with an equivalent cross-sectional area assigned through a nominal thickness, so as to reproduce the axial stiffness of the reinforcement. The first reinforcement layer was placed 0.25 m below the slope surface, followed by a second layer at a vertical spacing of 0.75 m. Subsequent layers were installed at 1.0 m vertical intervals down the slope. Reinforcement layer lengths were varied from 2.75 m to 6.25 m depending on depth, to ensure adequate embedment into the stable zone beyond the potential slip surface. These values were adopted as reasonable design assumptions, consistent with ranges reported in reinforced slope practice [13].

Vetiver roots were simulated using distributed truss elements, allowing only tensile resistance to be mobilized. A mean root diameter of 0.8 mm was adopted as a representative value. The corresponding root tensile strength and Young's modulus were defined using the empirical diameter-dependent relationships proposed in [14], where Equation (1) estimates tensile strength as a function of root diameter (D, mm) and Equation (2) provides the associated Young's modulus. A root area ratio (RAR) of 0.025% was selected within the experimentally reported range for Vetiver grass roots under landslide-affected and early growth conditions, as reported in [15]. For numerical modelling, the RAR was assumed to be uniformly distributed over the entire root depth as a simplifying assumption. As the empirical relationships were derived from tests conducted in clayey soils, a conservative reduction factor of 0.7 was applied to the computed root tensile strength to reflect the potentially weaker interaction between roots and silty soils. This value was selected to reflect a moderate reduction while avoiding excessive conservatism, consistent with common practice in parametric and numerical modelling where soil-specific calibration data are unavailable. The Young's modulus values were adopted without modification.

$$T_R = 15.239 \times D^{-0.893} \quad (1)$$

$$E_R = 342.74 \times D^{-1.399} \quad (2)$$

Where, T_R denotes the tensile strength (MPa), E_R represents Young's modulus (MPa), and D is the root diameter (mm).

All reinforcement elements were coupled to the soil using embedded-region constraints, a commonly adopted simplification for tensile reinforcements in numerical slope analyses.

F. Determination of factor of safety (Strength Reduction Method)

Slope stability was evaluated using the strength reduction method (SRM), in which the soil shear strength parameters are systematically reduced until numerical failure occurs. In this approach, the effective cohesion c' and the tangent of the effective friction angle $\tan\phi'$ are divided by a trial strength reduction factor F, such that

$$c'_r = \frac{c'}{F}, \qquad tan\ \phi'_r = \frac{tan\ \phi'}{F}$$

where c'_r and ϕ'_r are the reduced shear strength parameters. Failure was identified when the model showed numerical non-convergence or a sharp increase in displacement for a small increase in the strength reduction factor F. The value of F at failure was taken as the factor of safety. This method allows the failure mechanism to develop naturally within the finite element mesh without assuming a predefined slip surface. The procedure follows the concepts reported in [16] and [17], and is now standard practice in finite element slope stability analysis.

G. Validation of Model

The numerical model was verified by replicating the unsaturated slope case study presented in [18]. Their slope geometry, boundary conditions, and material properties were adopted directly, and the soil–water characteristic curve (SWCC) was digitized and interpreted from the published data. As the reference study did not report any external loading, only self-weight (gravity) was applied to represent the static condition of the slope.

The model was first brought to an initial equilibrium state before applying rainfall infiltration. Transient pore-pressure boundary conditions were imposed following the procedures described in [18]. The resulting pore-pressure responses and displacement showed trends consistent with those reported in the original study as shown in Fig. 4 and Fig. 5 respectively. Plastic equivalent strain (PEEQ) developed at the slope toe, which aligns with the failure initiation zone identified in [18]. Although the magnitude of PEEQ differed, the plastic zone remained confined to the same region. These differences are attributed to variations in mesh density, constitutive modelling, and interpretation of the SWCC data.

International Journal of Engineering Research & Technology (IJERT)
ISSN: 2278-0181
Vol. 14 Issue 12 , December - 2025

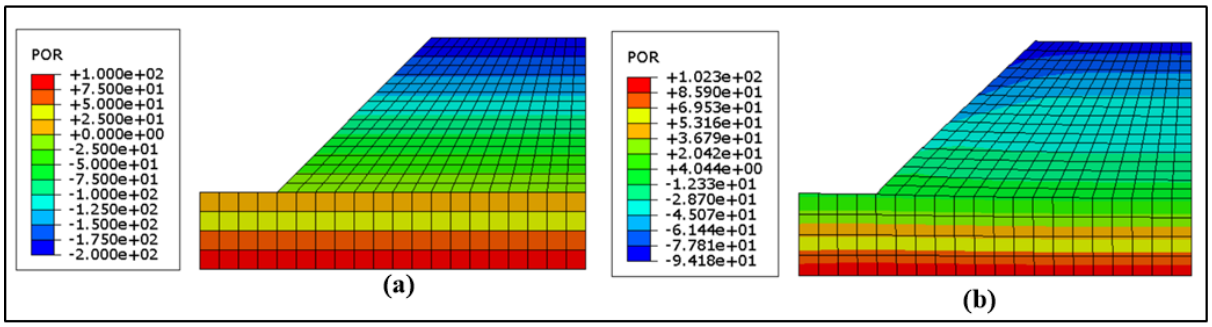

Fig. 4 Pore-water pressure distributions in the reproduced benchmark slope under initial conditions and after 72 h of rainfall infiltration

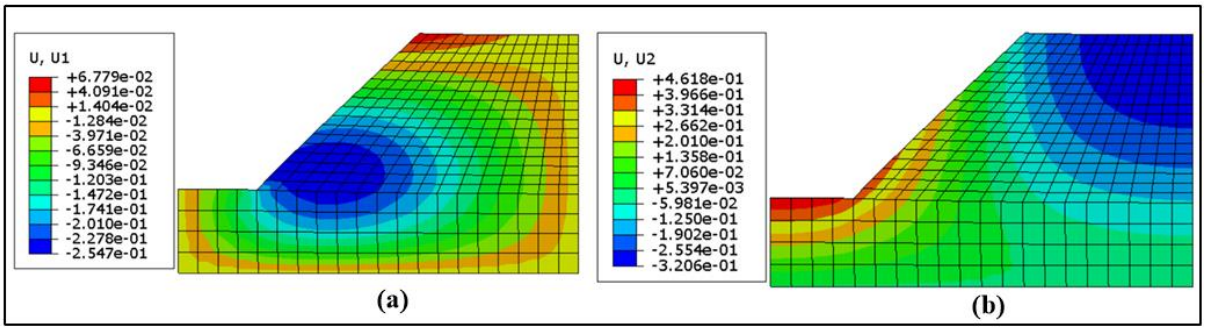

Fig. 5 Horizontal (U_1) and vertical (U_2) displacement contours of the benchmark slope reproduced for validation of the numerical model

Overall, the model reproduced the same failure mechanism and rainfall-induced behaviour as the reference case, demonstrating adequate accuracy for use in the subsequent analyses of both unreinforced and reinforced slopes.

III. RESULT AND DISCUSSIONS

A. Baseline slope

Fig. 6(a) shows the pore-pressure distribution prior to rainfall, with the slope remaining unsaturated and exhibiting high suction near the surface that gradually decreases with depth. In contrast, Fig. 6(b) illustrates the pore-pressure condition after 48 hours of rainfall infiltration, marked by a considerable reduction in suction near the surface and the development of a wetting front within the slope.

Fig. 7(a) corresponds to the pseudo-static loading under unsaturated conditions, where the initial matric suction is still present. In this case, the plastic equivalent strain (PEEQ) band develops along a shallower failure path, reflecting the higher apparent shear strength provided by suction. Whereas, Fig. 7(b) represents the pseudo-static loading combined with rainfall infiltration, where suction has been reduced due to wetting. Here, the PEEQ zone becomes more continuous and slightly deeper, indicating a weaker soil mass and a more pronounced tendency toward shear failure as rainfall reduces the effective strength.

The factor of safety is 1.15 under the pseudo-static unsaturated condition, and it further decreases to 1.10 when rainfall infiltration is introduced, as shown in Fig. 8.

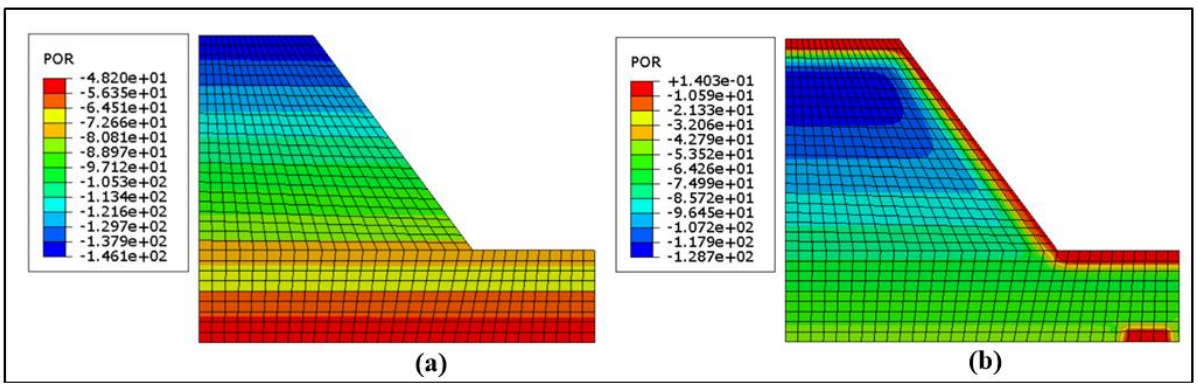

Fig. 6 Pore-water pressure distributions (a) before rainfall (b) after rainfall infiltration

International Journal of Engineering Research & Technology (IJERT)
ISSN: 2278-0181
Vol. 14 Issue 12 , December - 2025

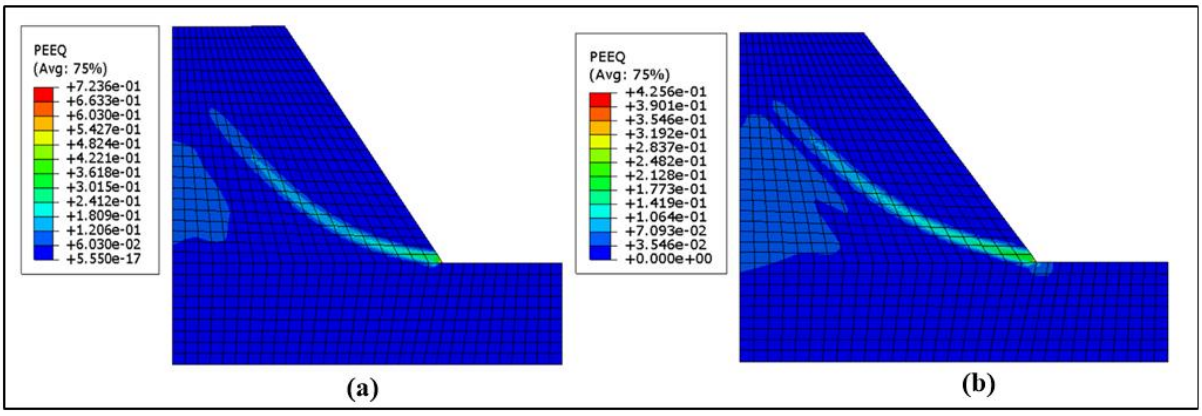

Fig. 7 Plastic strain (PEEQ) contours under pseudo-static loading for (a) unsaturated and (b) rainfall-influenced conditions

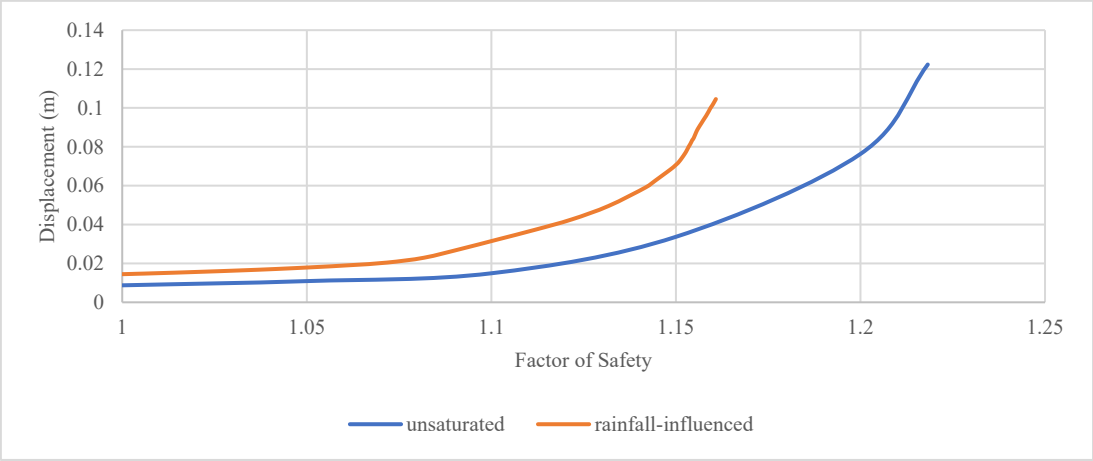

Fig. 8 Variation of displacement with factor of safety under pseudo-static loading for unsaturated and rainfall-influenced conditions

B. Slope Reinforced with Soil Nails

After validating the model for the baseline (unreinforced) slope, the same approach was used to analyse a soil-nailed slope. Soil nails were installed within the slope, as shown in Fig. 9, to examine how they improve the overall stability under the same boundary and loading conditions. The pore-pressure contours in Fig. 10(a) and Fig. 10(b) closely resemble the baseline state, indicating negligible hydraulic change and unchanged suction within the slope.

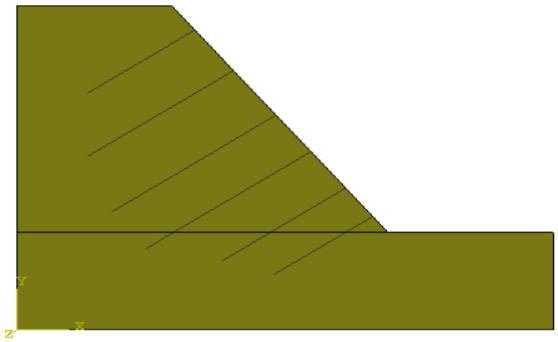

Fig. 9 Layout of soil nails within the slope

International Journal of Engineering Research & Technology (IJERT)
ISSN: 2278-0181
Vol. 14 Issue 12 , December - 2025

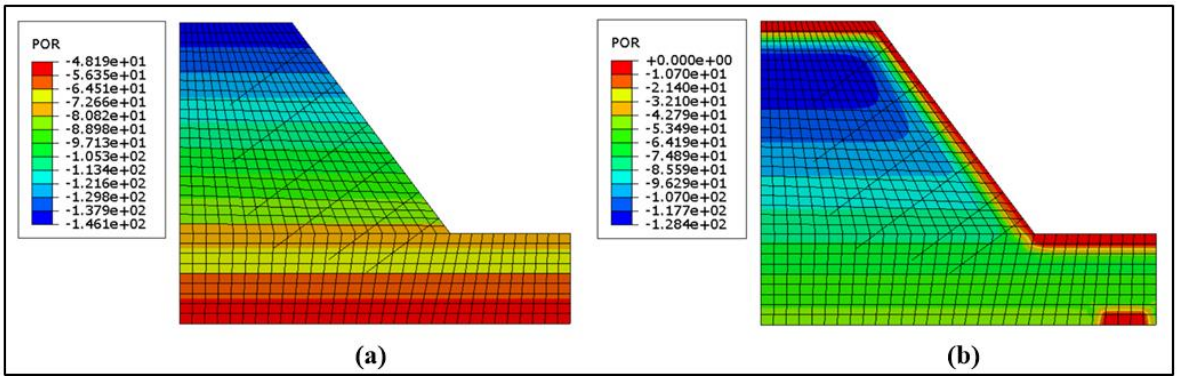

Fig. 10 Pore-water pressure distributions (a) before rainfall (b) after rainfall infiltration

Under unsaturated conditions, higher PEEQ magnitudes are observed because matric suction enhances the apparent shear strength of the soil, allowing greater stress mobilization prior to yielding. Once yielding initiates under pseudo-static loading, plastic strain localizes more distinctly along the failure zone as observed in Fig. 11 (a). After rainfall, the loss of suction reduces soil stiffness and strength, resulting in lower PEEQ values, while the overall failure pattern remains similar is shown in Fig. 11(b).

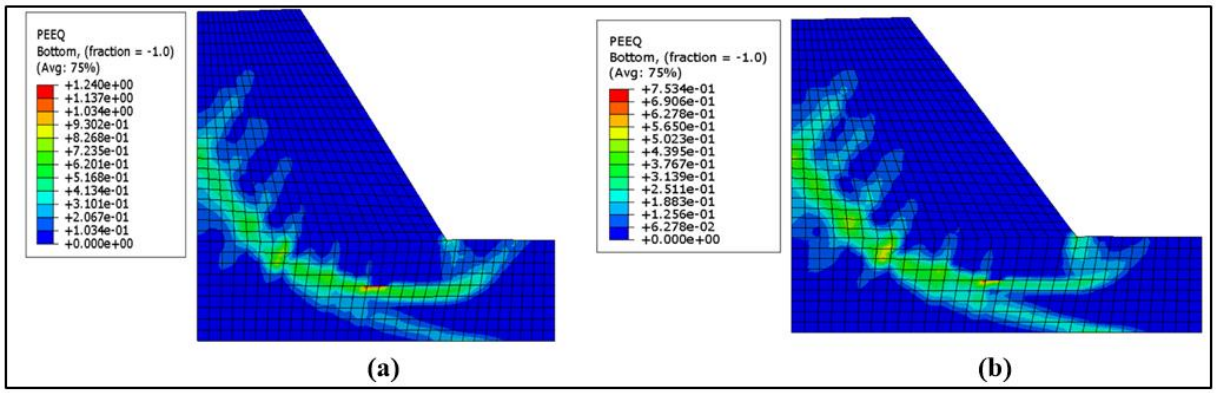

Fig. 11 Plastic strain (PEEQ) contours under pseudo-static loading for (a) unsaturated and (b) rainfall-influenced conditions

In Fig. 12, the factor of safety (FOS) is 1.45 under pseudo-static (unsaturated) conditions and declines slightly to 1.40 when pseudo-static loading is combined with rainfall, indicating that infiltration-driven changes in suction and pore-pressure partially reduce the slope's resistance to failure.

.

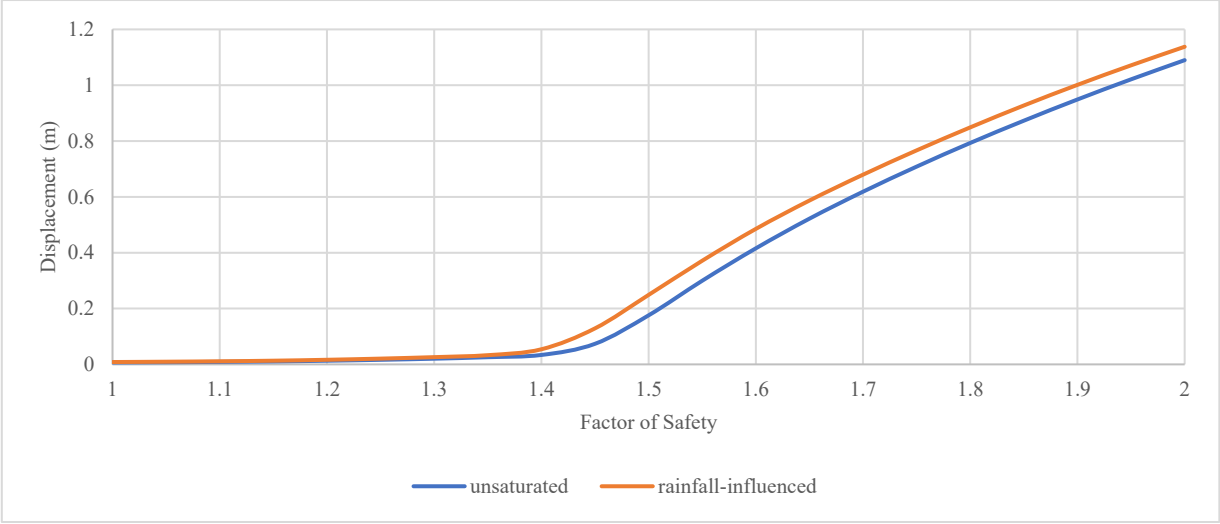

Fig. 12 Displacement–factor of safety response under unsaturated and rainfall-influenced conditions for pseudo-static loading

International Journal of Engineering Research & Technology (IJERT)
ISSN: 2278-0181
Vol. 14 Issue 12 , December - 2025

C. Slope Reinforced with Geogrid layers

The layout of the geogrid reinforcement adopted in the model is shown in Fig. 13, which was introduced to improve the stability of the slope relative to the baseline condition.

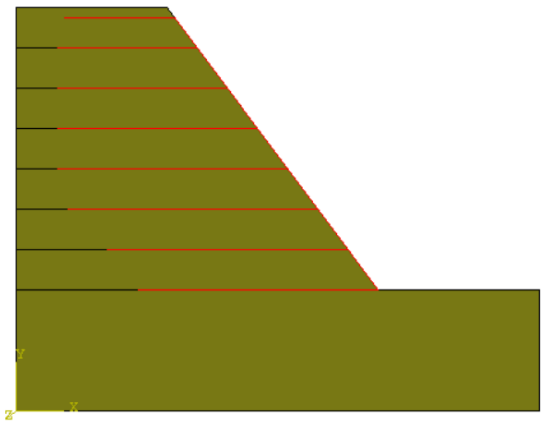

Fig. 13 Geogrid-reinforced slope showing the geogrid layout

Fig. 14 presents the pore-pressure distribution before and after rainfall. The response of the geogrid-reinforced slope differs noticeably from that of the baseline slope, particularly under rainfall conditions. A distinct pattern appears in which the reduction in suction penetrates deeper into the slope and along the reinforced base. This behaviour arises because the geogrid modifies the local stress and deformation fields, thereby influencing the pore-pressure evolution during infiltration.

Although both cases exhibit a similar overall failure mechanism, the pseudo-static unsaturated condition is presented in Fig. 15(a) shows a higher peak plastic strain, reflecting greater stress mobilization while matric suction is still present. Under rainfall conditions, the reduction in matric suction and the increase in pore-water pressures lead to earlier yielding and a slightly deeper extension of the plastic zone, although the peak PEEQ values are lower, as shown in Fig. 15(b). Despite these differences, in both cases the deformation remains largely confined within the reinforced region near the toe, reaffirming the role of the geogrid in limiting the progression of the shear zone.

The factor of safety shown in Fig. 16 is 1.45 under pseudo-static (unsaturated) loading and decreases slightly to 1.40 when rainfall is combined with pseudo-static loading, primarily due to the reduction in matric suction and the associated increase in pore-water pressures, which lowers the soil's effective strength.

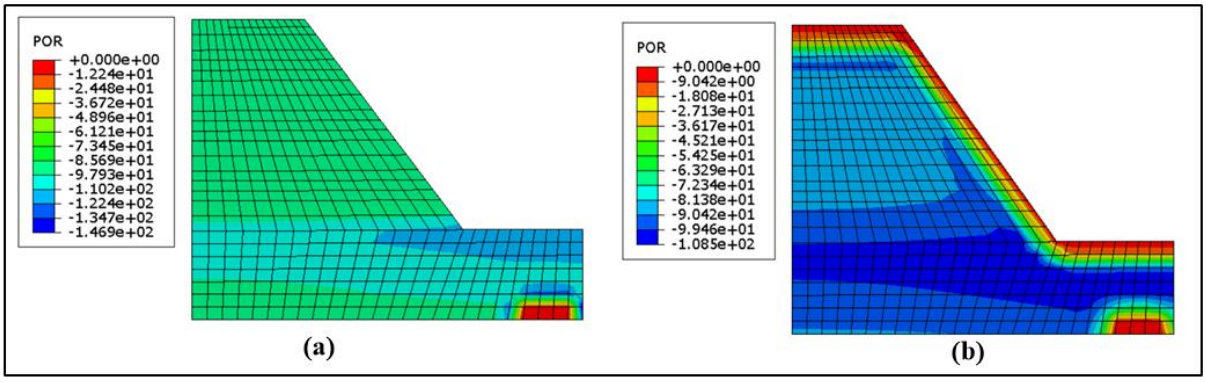

Fig. 14 Pore-water pressure distributions (a) before rainfall (b) after rainfall infiltration

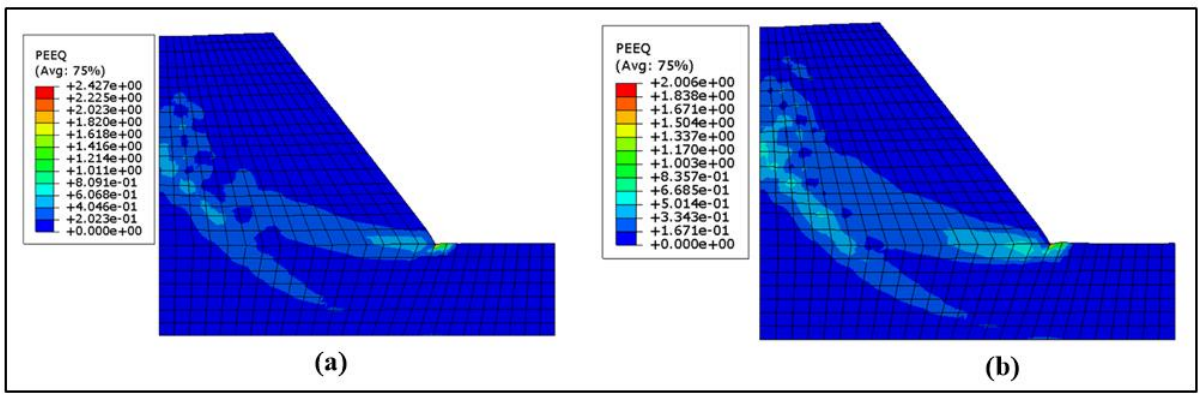

Fig. 15 Plastic strain (PEEQ) contours under pseudo-static loading for (a) unsaturated and (b) rainfall-influenced conditions

International Journal of Engineering Research & Technology (IJERT)
ISSN: 2278-0181
Vol. 14 Issue 12 , December - 2025

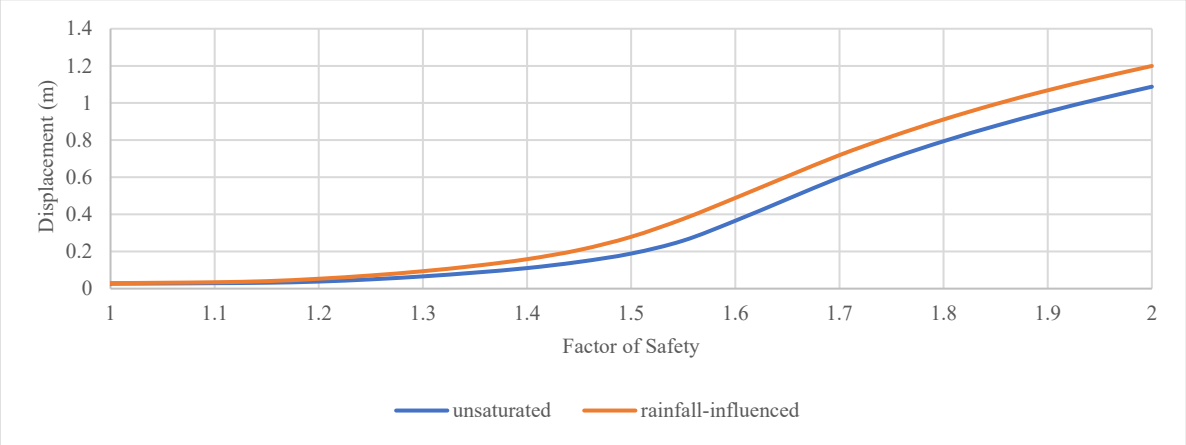

Fig. 16 Displacement–factor of safety response under pseudo-static loading for unsaturated and rainfall-influenced conditions

D. Soil Reinforced with Vetiver roots

The vetiver root adopted in the soil slope is shown in Fig. 17. As shown in Fig. 18(a) and (b), the pore-pressure patterns differ very little from the baseline, indicating that the presence of vetiver roots does not significantly alter the hydraulic behaviour within the slope. In the pseudo-static unsaturated case, as shown in Fig. 19(a) the slope exhibits a localized higher peak PEEQ value near the toe, while plastic strain elsewhere remains relatively low and distributed over a broader area. In contrast, under pseudo-static rainfall conditions, the peak PEEQ value is lower; however, the plastic strain zone becomes more continuous, extends deeper, and propagates further upslope along the potential slip surface as shown in Fig. 19(b). This occurs because rainfall reduces matric suction and increases pore-water pressure, causing plastic deformation to develop over a larger portion of the slope even at lower strain levels.

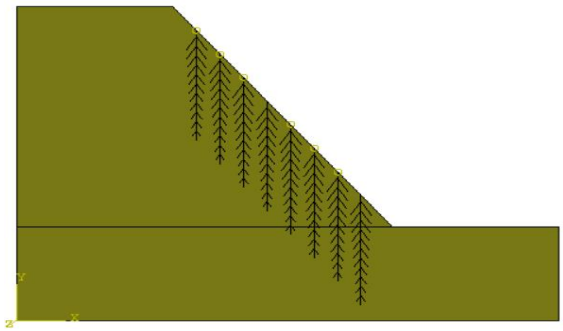

Fig. 17 Vetiver root layout within the slope

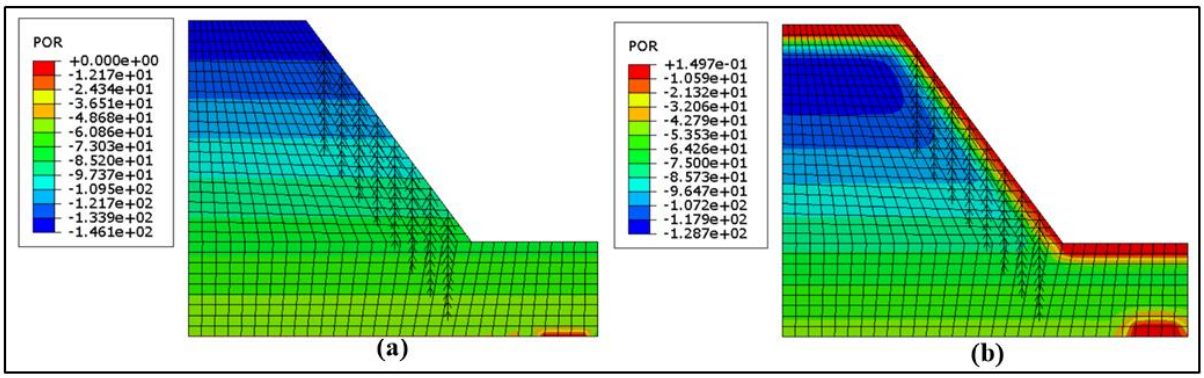

Fig. 18 Pore-water pressure distributions (a) before rainfall (b) after rainfall infiltration

International Journal of Engineering Research & Technology (IJERT)
ISSN: 2278-0181
Vol. 14 Issue 12 , December - 2025

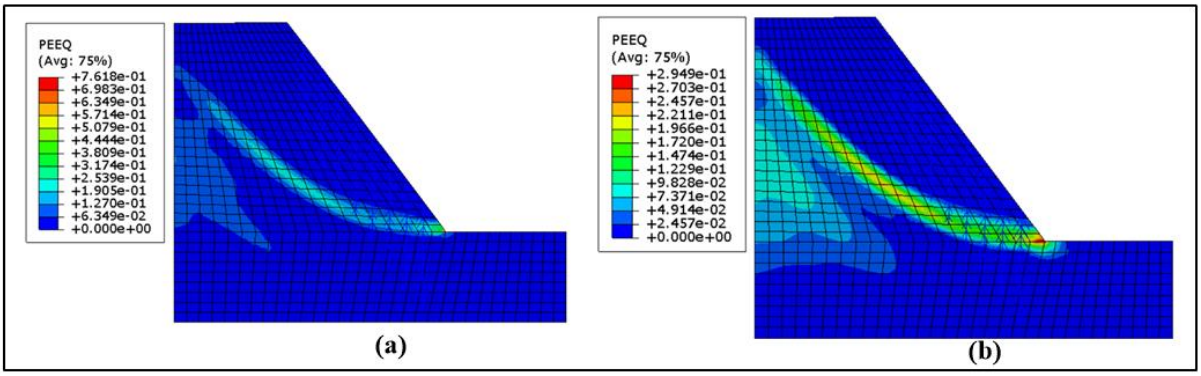

Fig. 19 Plastic strain (PEEQ) contours under pseudo-static loading for (a) unsaturated and (b) rainfall-influenced conditions

Fig. 20 illustrates that slope stability reduces under the combined effects of rainfall and seismic loading. The pseudo-static unsaturated case reaches a FOS of 1.20, whereas the pseudo-static rainfall condition yields the lowest value at 1.15, indicating a limited margin of safety.

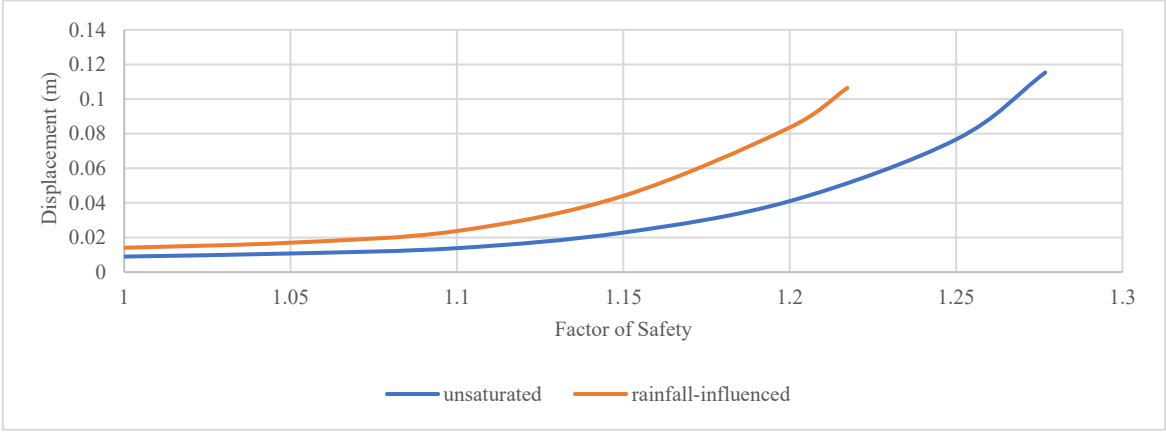

Fig. 20 Displacement–factor of safety response under pseudo-static loading for unsaturated and rainfall-influenced conditions

E. Comparative Displacement Behaviours (Critical Case)

Fig. 21 shows the horizontal displacement contours for all slope configurations under the critical pseudo-static–rainfall condition at their respective Factors of Safety. The baseline slope (a) develops a small and shallow deformation zone near the surface, indicating the early stage of failure, consistent with the sharp increase in horizontal displacement used to identify the critical Factor of Safety in the SRM approach. The nail-reinforced slope (b) exhibits a deeper and more distributed deformation zone compared to the baseline case, reflecting the mobilization of nail and soil interaction that transfers loads into the stable interior of the slope and promotes a deeper failure mechanism. The geogrid-reinforced slope (c) has a more confined and narrower deformation zone, especially when compared to the wider zones in (a) and (b). This localized pattern reflects the geogrid's ability to restrict lateral deformation and provide effective confinement within the reinforced region. The vetiver-reinforced slope (d) shows a moderately wide deformation zone extending toward the slope face and toe, indicating improved control of shallow movements associated with root reinforcement.

Although the absolute displacement magnitudes are not directly comparable because each configuration is plotted at its own critical Factor of Safety, the deformation patterns collectively indicate that all reinforcement types enhance stability, with structural systems providing deeper confinement and vegetation offering an effective and sustainable solution for shallow stabilization.

Fig. 22 illustrate the vertical displacement contours for all slope configurations under the critical pseudo-static rainfall condition at their respective Factors of Safety. The baseline slope (a) shows only minor crest settlement, indicating the onset of shallow deformation. In contrast, the nail-reinforced slope (b) exhibits a more pronounced and slightly deeper crest settlement band, reflecting mobilization of shear resistance within the reinforced zone and redistribution of deformation toward the slope crest as lateral movement is restrained. The geogrid-reinforced slope (c) exhibits the largest localized crest settlement, reflecting strain concentration near the upper ends of the stiff reinforcement layers. By limiting lateral spreading, the geogrids promote vertical adjustment that becomes more evident near the crest.

International Journal of Engineering Research & Technology (IJERT)
ISSN: 2278-0181
Vol. 14 Issue 12 , December - 2025

The vetiver-reinforced slope (d) exhibits limited and diffuse crest settlement, indicating an indirect reduction in crest deformation due to root reinforcement concentrated along the slope face and shallow subsurface. Overall, although the reinforced slopes exhibit larger localized crest settlements, the deformation remains confined and represents strain redistribution rather than global instability.

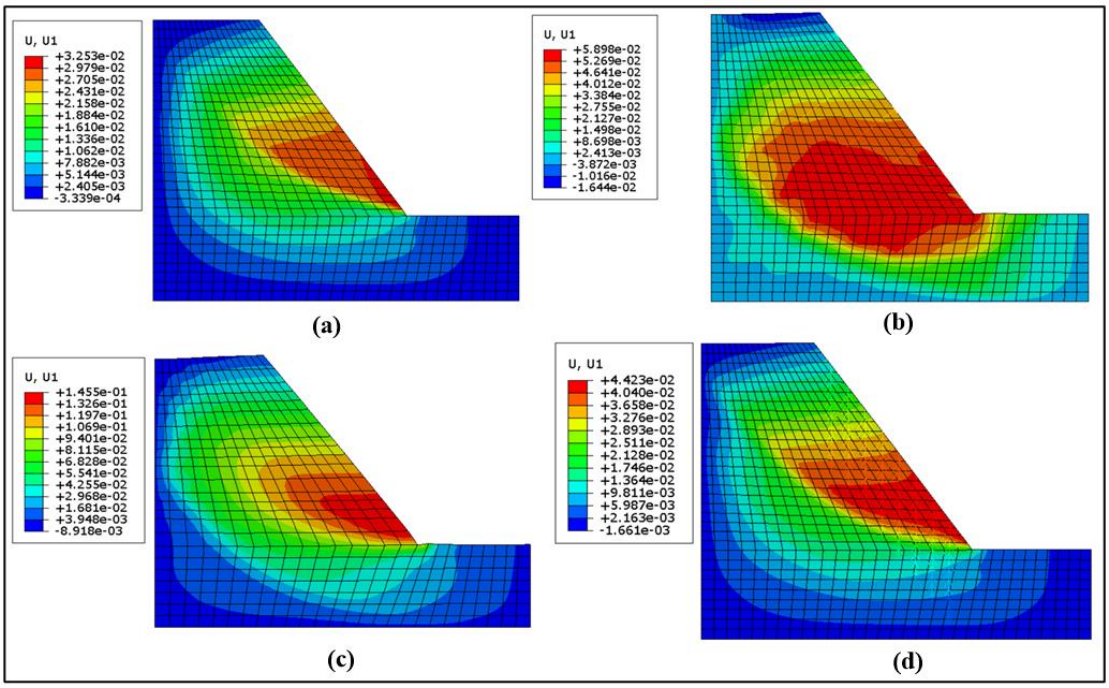

Fig. 21 Horizontal displacement contours at the respective FOS under pseudo-static rainfall-influenced conditions for (a) baseline, (b) soil-nailed, (c) geogrid, and (d) vetiver-reinforced slope

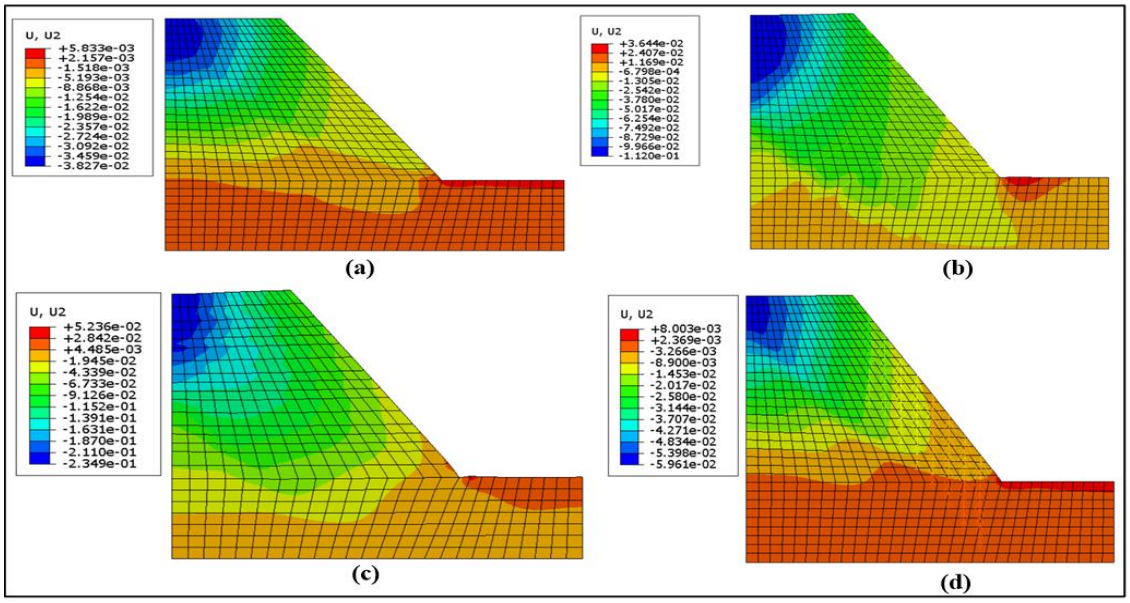

Fig. 22 Vertical displacement contours at the respective FOS under pseudo-static rainfall-influenced conditions for (a) baseline, (b) soil-nailed, (c) geogrid, and (d) vetiver-reinforced slope

International Journal of Engineering Research & Technology (IJERT)
ISSN: 2278-0181
Vol. 14 Issue 12 , December - 2025

F. Comparison of Factor of Safety

Fig. 23 presents that under pseudo-static unsaturated loading, both soil nails and geogrids produce a 26.09% increase in the FOS relative to the baseline slope, demonstrating strong and comparable reinforcement effects, while vetiver roots contribute a modest 4.35% improvement. Under rainfall-influenced conditions, the relative improvement provided by nails and geogrids increases slightly to 27.27%, indicating that their stabilizing performance remains effective despite the reduction in matric suction. Vetiver roots exhibit a small increase in relative improvement to 4.55% under rainfall conditions, reflecting a limited but consistent enhancement of slope stability.

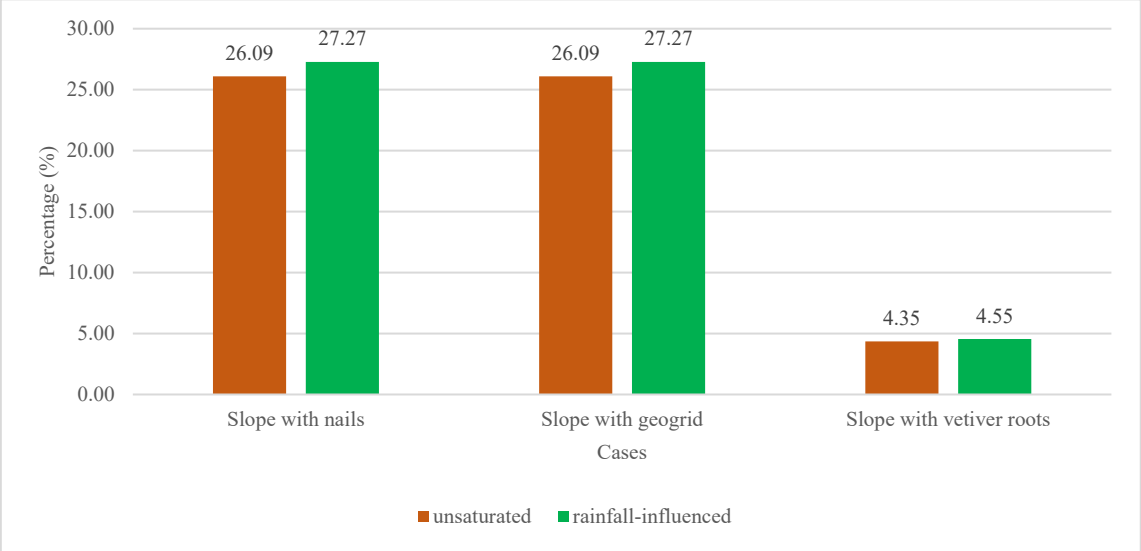

Fig. 23 Percentage improvement in FOS for different slope reinforcement systems under unsaturated and rainfall-influenced conditions

IV. CONCLUSIONS

1. Under the pseudo-static loading, both the nail reinforced and the geogrid reinforced slopes showed equal improvement in FOS over the baseline condition, with values of approximately 26.1% under unsaturated case and 27.3% under rainfall-influenced condition, while the vetiver reinforced slope showed only small values of approximately 4.4% and 4.6% in the FOS improvement for unsaturated and rainfall-influenced states respectively, highlighting the much stronger effect of structural reinforcements.
2. The horizontal displacement behaviour indicates that the different reinforcement systems develop more defined and organized deformation patterns compared to the baseline slope, reflecting a more stable distribution of lateral movements under pseudo-static conditions.
3. Vertical displacement behaviour shows that each slope configuration develops a distinct crest-settlement pattern, with the reinforced slopes forming more localized deformation zones than the baseline case. These differences reflect the characteristic deformation response of each system under pseudo-static conditions.
4. Plastic strain (PEEQ) patterns indicate that reinforcement promotes more favourable failure mechanisms compared to the shallow slip observed in the baseline slope. The nail and geogrid systems develop deeper, more distributed plastic zones, while the vetiver system forms a continuous and clearly developed plastic band. Overall, all reinforcement types contribute to a more stable and controlled deformation response under pseudo-static loading.
5. The pore-pressure response under rainfall shows that the applied drainage boundary effectively dissipated infiltrated water and prevented excessive positive pore-pressure buildup, supporting a more stable hydraulic condition within the slope during analysis.
6. The overall findings demonstrate that soil nails and geogrid reinforcement provide greater stability improvement, while vetiver roots offer a sustainable, resource-efficient option for shallow slopes, highlighting the practical applicability of these techniques under pseudo-static conditions.

International Journal of Engineering Research & Technology (IJERT)
ISSN: 2278-0181
Vol. 14 Issue 12 , December - 2025

V. REFERENCES

[1] A. N. C. Ghani, A. Mohd Taib, and D. Z. Abang Hasbollah, "Effect of rainfall pattern on slope stability," in *Geotechnics for sustainable infrastructure development*, P. Duc Long and N. T. Dung, Eds., Lecture Notes in Civil Engineering, vol. 62, Singapore: Springer, pp. 887–892, 2020.

[2] S. L. Kramer, *Geotechnical earthquake engineering*, New Jersey, USA: Prentice Hall, 1996.

[3] D. V. Griffiths, "Slope stability analysis using finite elements," *The Open Geotechnical Journal*, vol. 9, pp. 1–14, 2015.

[4] A. W. Bishop, "The principle of effective stress," *Teknisk Ukeblad*, vol. 39, pp. 859–863, 1959.

[5] S. K. Vanapalli, D. G. Fredlund, D. E. Pufahl, and A. W. Clifton, "Model for the prediction of shear strength with respect to soil suction," *Canadian Geotechnical Journal*, vol. 33, no. 3, pp. 379–392, 1996.

[6] P. Pichler and H. F. Schweiger, "Numerical analysis of the stability of inhomogeneous slopes considering partially saturated conditions," *E3S Web of Conferences*, vol. 9, art. no. 15010, 2016.

[7] Indian Roads Congress, *IRC:6–2017: Standard specifications and code of practice for road bridges, Section II—Loads and load combinations*, New Delhi, India: IRC, 2017.

[8] Bureau of Indian Standards, *IS 1893 (Part 1): Criteria for earthquake resistant design of structures—General provisions and buildings*, New Delhi, India: BIS, 2016.

[9] S. Liu, L. Shao, and H. Li, "Pseudo-static and dynamic stability analysis of slopes under seismic loading," *Soil Dynamics and Earthquake Engineering*, vol. 120, pp. 292–302, 2019.

[10] S. Povraz and S. Vural, "Parametric investigation of corner effect on soil-nailed support systems of deep excavations," *Applied Sciences*, vol. 14, no. 4, art. no. 7331, 2024.

[11] M. Al-Bargawi, R. Aqel, M. Wayne, H. Titi, and R. Elhajjar, "Polymer geogrids: A review of material, design and structure relationships," *Materials*, vol. 14, no. 16, art. no. 4745, 2021.

[12] R. M. Koerner, *Designing with geosynthetics*, 6th ed., Xlibris Corporation, 2012.

[13] R. Zhang, M. Long, T. Lan, J. Zheng, and G. Chao, "Stability analysis method of geogrid reinforced expansive soil slopes and its engineering application," *Journal of Central South University*, vol. 27, no. 7, pp. 1965–1980, 2020.

[14] C. Teerawattanasuk, J. Maneecharoen, D. T. Bergado, P. Voottipruex, and L. G. Lam, "Root strength measurements of Vetiver and Ruzi grasses," *Lowland Technology International*, vol. 16, no. 2, pp. 71–80, 2014.

[15] Y. A. Fata, H. Hendrayanto, S. D. Tarigan, and C. Wibowo, "Vetiver root cohesion at different growth sites in Bogor, Indonesia," *Biodiversitas*, vol. 23, no. 3, pp. 1683–1692, 2022.

[16] E. M. Dawson, W. H. Roth, and A. Drescher, "Slope stability analysis by strength reduction," *Géotechnique*, vol. 49, no. 6, pp. 835–840, 1999.

[17] D. V. Griffiths and P. A. Lane, "Slope stability analysis by finite elements," *Géotechnique*, vol. 49, no. 3, pp. 387–403, 1999.

[18] R.-F. Zhou, X.-W. Lei, Q.-S. Meng, and C. Lin, "Stability analysis of unsaturated soil slopes under rainfall infiltration," *Advanced Materials Research*, vols. 594–597, pp. 126–129, 2012.